HHS Public Access

Author manuscript

Mol Cancer Res. Author manuscript; available in PMC 2022 January 01.

Published in final edited form as:

Mol Cancer Res. 2021 July ; 19(7): 1099–1112. doi:10.1158/1541-7786.MCR-20-0080.

Kinetic Characterization of ASXL1/2-Mediated Allosteric Regulation of the BAP1 Deubiquitinase

Hongzhuang Peng[1,*], **Joel Cassel**[1], **Daniel S. McCracken**[1,2], **Jeremy W. Prokop**[3,4], **Eleonora Sementino**[5], **Mitchell Cheung**[5], **Paul R. Collop**[6], **Alexander Polo**[1], **Surbhi Joshi**[1], **Jacob P. Mandell**[1], **Kasirajan Ayyanathan**[1], **David Hinds**[3,4], **S. Bruce Malkowicz**[7], **J. William Harbour**[8], **Anne M. Bowcock**[9], **Joseph Salvino**[1], **Eileen J. Kennedy**[6], **Joseph R. Testa**[5,*], **Frank J. Rauscher III**[1]

[1]The Wistar Institute, Philadelphia, Pennsylvania.

[2]Department of Biochemistry and Molecular Biophysics, University of Pennsylvania, Philadelphia, Pennsylvania.

[3]Department of Pediatrics and Human Development, College of Human Medicine, Michigan State University, Grand Rapids, Michigan.

[4]Department of Pharmacology and Toxicology, Michigan State University, East Lansing, Michigan.

[5]Fox Chase Cancer Center, Philadelphia, Pennsylvania.

[6]Department of Pharmaceutical and Biomedical Sciences, College of Pharmacy, University of Georgia, Athens, Georgia.

[7]Department of Surgery, University of Pennsylvania, Philadelphia, Pennsylvania.

[8]University of Miami School of Medicine, Miami, Florida 33101.

[9]Icahn School of Medicine at Mount Sinai, New York, New York.

Abstract

BAP1 is an ubiquitin hydrolase whose deubiquitinase activity is mediated by polycomb group-like protein ASXL2. Cancer-related *BAP1* mutations/deletions lead to loss-of-function by targeting the catalytic (UCH) or ULD domains of BAP1, and the latter disrupts binding to ASXL2, an obligate partner for BAP1 enzymatic activity. However, the biochemical and biophysical properties of domains involved in forming the enzymatically active complex are unknown. Here, we report the molecular dynamics, kinetics and stoichiometry of these interactions. We demonstrate that interactions between BAP1 and ASXL2 are direct, specific, and stable to biochemical and biophysical manipulations as detected by isothermal titration calorimetry, GST association, and optical biosensor assays. Association of the ASXL2-AB box greatly stimulates BAP1 activity. A stable ternary complex is formed, comprised of the BAP1-UCH, BAP1-ULD, and ASXL2-AB

[*]Corresponding authors: Hongzhuang Peng, The Wistar Institute, Philadelphia, PA 19104. Phone: 484-680-2804; h ongzhuangpeng851@gmail.com or Joseph R. Testa, Fox Chase Cancer Center, Philadelphia, PA 19111. Phone: 215-728-2610; joseph.testa@fccc.edu.

JRT and MC have a patent on *BAP1* mutation testing, and JRT has provided legal consultation regarding the role of germline mutations of *BAP1* in mesothelioma. The other authors declare no conflicts of interest.

domains. Stoichiometric analysis revealed that one molecule of the ULD domain directly interacts with one molecule of the AB box. Real-time kinetic analysis of the ULD/AB protein complex to the BAP1 UCH domain, based on SPR, indicated that formation of the ULD/AB complex with the UCH domain is a single-step event with fast association and slow dissociation rates. *In vitro* experiments validated in cells that ASXL-AB box directly regulates BAP1 activity.

Keywords

Deubiquitination; allosteric regulation; cancer biology; protein-protein interaction kinetics; structural model

Introduction

The BAP1 tumor suppressor is an ubiquitin hydrolase shown to associate with the RING finger motif of BRCA1 to augment BRCA1-mediated inhibition of breast cancer cell proliferation (1). The amino-terminus of BAP1 is comprised of an ubiquitin C-terminal hydrolase (UCH) domain that cleaves ubiquitin from ubiquitin-conjugated small substrates. BAP1 harbors binding motifs for both BARD1 and BRCA1, which form a heterodimer (2), and for a HCF1 binding site that networks with a histone-modifying complex during cell division (3). The carboxy-terminus of BAP1 consists of two nuclear localization signals and an UCH37-like domain (ULD). The ULD associates with ASXL family members to create the polycomb group (PcG)-repressive deubiquitinase complex, which plays a role in stem cell pluripotency and development (4,5).

Homology of the BAP1-UCH and other UCH-like proteins infers that this BAP1 motif functions in either ubiquitin-mediated, proteasomal degradation or some other ubiquitin-facilitated regulatory pathways that are involved in BRCA1 function, cellular proliferation, differentiation, and/or homeostatic processes (1,6,7). BAP1 has been found to act as a tumor suppressor both *in vitro* (1,2) and *in vivo* (8). Somatic mutations and exonic deletions of *BAP1* are frequently seen in metastatic uveal melanomas, malignant mesotheliomas, and other tumor types (9–11). Moreover, germline mutations of *BAP1* have been shown to predispose carriers to mesothelioma, uveal melanoma, benign and malignant cutaneous melanocytic tumors, basal cell carcinoma, meningioma, and renal carcinoma (11–15). Cancer-related mutations/deletions of *BAP1* often result in loss-of-function by causing premature protein termination and/or diminished UCH catalytic activity. Other *BAP1* mutations lead to loss-of-function by targeting the ULD domain, thereby disrupting binding to ASXL2 (16), an obligate partner for BAP1 enzymatic activity.

BAP1 interacts with ASXL family members as components of a large polycomb-like complex throughout vertebrate and invertebrate biology (5). BAP1 is homologous to a *Drosophila* protein known as Calypso. This *Drosophila* protein works together with the PcG protein ASX, and the resulting Polycomb repressive deubiquitinase (PR-DUB) complex then binds to specific PcG target genes. ASXL1/2/3 represent the human homologs of *Drosophila* ASX (16). The highly conserved ASX homology domain (ASXH) resides at the amino-terminus of ASXL and is essential for binding to Calypso/BAP1. Like *Drosophila* ASX-Calypso, human ASXL1/2/3-BAP1 deubiquitinates histone H2A. Recurrent inactivating

ASXL1/2/3 mutations leading to protein truncations have been found in human cancers and other diseases (17–20). For example, inactivating mutations of *ASXL1* in myeloid malignancies result in loss of polycomb repressive complex 2 (PRC2)-mediated transcriptional repression of leukemogenic target genes (17). Crystal structure studies of the *Drosophila* PR-DUB have demonstrated that the deubiquinase Calypso and ASX form a 2:2 complex. This ASX-Calypso complex is formed by dimerization of two activated Calypso proteins, and disruption of the Calypso dimer interface prevents the removal of H2AK119Ub as a consequence of compromised recruitment to nucleosomes (21).

In previous work, we showed that familial and somatic *BAP1* mutations inactivate ASXL1/2-mediated allosteric regulation of the BAP1 deubiquitinase by targeting multiple independent domains (16). Furthermore, our biochemical work demonstrated that the ASXL2-AB box binds to the BAP1-ULD domain, but not to BAP1-UCH. As a consequence, a tripartite complex is formed consisting of AB, ULD, and UCH. Binding of the AB box to ULD then stabilizes the BAP1-UCH and increases its catalytic activity. Tumor-derived in-frame mutations occurring outside of the BAP1-UCH domain disrupt the interaction between BAP1 and ASXL2, leading to loss of BAP1 catalytic activity. In the present investigation, we define the biochemical and biophysical properties of the domain-domain interactions of this complex, focusing on the molecular dynamics, kinetics and stoichiometry of these interactions. We also perform experiments in human cells that validate the interactions between BAP1 and ASXL2, including that the ASXL-AB domain directly regulates BAP1 deubiquitinase activity. Importantly, these new studies elucidate the molecular dynamics of these interactions, measure the kinetic and stoichiometric impact of mutations on protein binding and on the enzymatic activity of BAP1, and provide novel insights about the structural and dynamic parameters of the BAP1-ASXL2 interaction into single cell datasets that can inform future small-molecule approaches designed to reactivate latent wild-type UCH activity in *BAP1*-mutant malignancies.

Materials and methods

Plasmids

The pFastBacTHa-BAP1-FL-WT, -BAP1-UCH-WT and -UCH-C91S mutant plasmids, pGEX-2TK-BAP1-UCH-WT (1–250 aa), pGEX-4T-1-BAP1-ULD, pQE30-BAP1-ULD (601–729aa) and pQE30-ASXL2-AB (261–381aa) plasmids were previously described (16). The pETDuet-1-His-BAP1-ULD+ASXL2-AB plasmid was constructed through PCR-based cloning and was sequenced to confirm its authenticity.

Proteins expression and purification

The baculovirus (Bv) Bv-His-BAP1-FL-WT, Bv-His-BAP-UCH-WT and Bv-UCH-C91S mutant proteins were expressed in Bv-infected Sf9 cells and purified as described (16). The GST- and His-tagged BAP1 and ASXL2 proteins were expressed in *E. coli* BL21 (DE3) (Stratagene) and SG13009 (S9) (Qiagen), respectively. The pETDuet-1-His-BAP1-ULD +ASXL2-AB protein complex was expressed in Rosetta 2 (DE3) pLysS (Millipore). Bacteria bearing the desired plasmids were propagated with aeration at 37°C in 1L of 2YT to an A_{600}

absorbance of approximately 0.6. IPTG was added to 1 mM, and growth was continued at 20°C overnight. Cells were harvested by centrifugation.

GST-fusion proteins were purified as described previously (22). Bacterial His-tagged proteins were purified under denaturing conditions (Qiagen) and then refolded by dialysis as described (22). The recombinant human BAP1-FL-WT protein was purchased from Boston Biochem (E-345–050). The Duet-His-ULD/AB protein complex was purified under native purification conditions using Cobalt beads (Talon), followed by dialysis to desired concentration.

GST association assays

GST association assays were performed as described (23) using BB200 buffer (200 mM NaCl, 20 mM Tris, pH 7.5, 0.2 mM EDTA, 10% Glycerol, 1 mM PMSF and 0.2% NP40) and BB500 (containing the same components as BB200 except that the concentration of NaCl was 500 mM).

Dynamic light scattering (DLS)

DLS was measured using DynaPro Titan (Wyatt Technology). Purified His-BAP1-ULD, His-AB and His-ULD/AB complex were in buffer containing 50 mM potassium phosphate, pH 7.5, 200 mM KCl and 1mM TCEP. His-ULD was measured at 574 μM concentration, His-AB was measured at 77 μM concentration, and His-ULD/AB protein complex was measured at 70 μM concentration. Samples were microcentrifuged at 13,000 rpm for 10 min prior to measurements at 10°C.

Isothermal titration calorimetry (ITC)

ITC was performed using Microcal ITC 200 (Microcal/Malvern Instruments). His-ULD and His-AB proteins were dialyzed in 50 mM potassium phosphate, pH 7.5, 200 mM potassium chloride, and 1 mM TCEP. His-AB was placed in the sample cell at concentration 77 μM. His-ULD was titrated into the sample cell at a concentration of 574 μM. Two references were used. The first reference was titration of the buffer into His-AB protein. The second was titration of His-ULD protein into the buffer. Both reference values were subtracted from the experimental data. ITC calculations and fitting were performed with Origin 7 software, using autofit, 200 iterations. Based on the results, stoichiometry and binding kinetics of the proteins were determined. Direct measurements of binding affinity (K_a), enthalpy changes (ΔH) and binding stoichiometry (n) were used to determine the Gibbs free energy changes (ΔG) and entropy changes (ΔS) using $\Delta G = -RT\ln K_a = \Delta H - T\Delta S$ (R = gas constant; T = absolute temperature). Dissociation constant (K_d) is $1/K_a$. Experiments were performed in duplicate. No uncertainty ranges are given due to the low number of technical replicates.

Circular Dichroism (CD)

CD spectra (190–260 nm) were measured on a Jasco J-715 spectropolarimeter (Japan Spectroscopic) at 25°C. The CD spectra were recorded using 0.1 cm path length quartz cuvettes with the following measurement parameters: 190–260 nm; step resolution: 1 nm; speed: 20 nm/min; accumulations: 4; bandwidth: 1 nm. All measurements were performed in

the following buffer: 50 mM potassium-phosphate, pH 7.5, 300 mM KCl, 10% glycerol, 1 mM DTT and 1 mM PMSF. Data were processed using Jasco Spectra Manager Suite.

Ub-AMC assay

The activity of BAP1 or BAP1-UCH proteins was determined by cleavage of ubiquitin-7-amido-4-methylcoumarin (Ub-AMC). Assays contained various concentrations of enzyme and substrate with and without His-AB or the His-ULD/AB complex as indicated in the figures in a reaction volume of 15 uL of 25 mM HEPES, pH 7.4, 150 mM NaCl, 5 mM DTT, 0.005% Tween20 in low-volume 384-well plates at room temperature. Fluorescence of free AMC at excitation and emission wavelengths of 355 nm and 460 nm, respectively, was measured at 2-min intervals for 20 min in an Envision microplate reader. Background fluorescence in the absence of enzyme was subtracted from the data points, and the linear portion of the curve was fit to a straight line to determine velocity.

Kinetic analysis: surface plasmon resonance (SPR)

Interactions between ASXL-AB and BAP1-ULD domains were studied by SPR using a Biacore T200 instrument. GST-antibody (Abcam ab9085) was coupled to all flow cells of a CM5 sensor chip using standard amine coupling procedures in HEPES-buffered saline running buffer. After coupling of the GST antibody, the running buffer was changed to 25 mM HEPES, pH 7.4, 150 mM NaCl, 5 mM DTT and 0.05% Tween20. GST-ULD was immobilized onto the chip surface at a ligand density of 400 RU, followed by a 120-s stabilization period. A single concentration His-AB was then injected over both the reference cell, with GST antibody alone, and the flow cell covered with GST-ULD at 30 uL/min. The binding reaction was monitored for 240 s followed by a 300-s dissociation time. Specific binding was determined by subtracting the refractive index change in the reference cell from the flow cell containing GST-ULD. After each concentration of His-AB, the GST-ULD was stripped from the surface using a 60-s injection of 20 mM glycine, pH 2.0 at 30 uL/min, followed by another 120-s stabilization period. Fresh GST-ULD was then immobilized as above. Experiments were done in triplicate.

Interactions between the His-ULD/AB complex and full-length BAP1 or the BAP1-UCH domain were also studied using the Biacore T200 instrument. Full-length His-BAP1, GST-UCH, or GST alone was directly immobilized to a CM5 sensor chip at a density of ~3000 RU using standard amine coupling procedures. The running buffer for the binding studies was 25 mM HEPES, pH 7.4, 250 mM NaCl, 5 mM DTT and 0.05% Tween20. The higher NaCl concentration was required to reduce nonspecific binding to the reference cell in the absence of protein. Various concentrations of His-ULD/AB complex were injected over flow cells at 30 uL/min, and the binding reaction was monitored for 90 s followed by a 240-s dissociation time. Specific binding was determined by subtracting the refractive index change in the reference cell from the readings of the other three flow cells. After the 240-s dissociation time, most of the His-ULD/AB complex was completely dissociated. However, 1 M NaCl at 30 uL/min was injected for 60 s over the flow cells to clear any remaining bound protein. Experiments were done in triplicate.

Sequence and structure analysis

Open reading frame sequences for *BAP1*, *UCHL1*, *UCHL3*, *UCHL5*, *ASXL1*, *ASXL2*, and *ASXL3* were obtained from NCBI for vertebrate species. Separately, *UCH* or *ASX* sequences were aligned and codon selection scored using our previously published metrics (24). COSMIC variants (25) for *BAP1* were extracted on June 20, 2018. Secondary structure predictions for proteins were performed using http://cib.cf.ocha.ac.jp/bitool/MIX/ and a combination of Chou-Fasman, GOR, and Neural Network predictions. Conservation was highlighted onto the human protein model generated from PDB 6cga.

Co-Immunoprecipitation (Co-IP) and immunoblot analysis

Interactions between the BAP1-UCH and BAP1-ULD proteins and the ASXL2-AB box (261–649 aa) protein *in vitro* were determined by IP-Western blotting (IP-WB). HEK 293T cells were transiently transfected using Lipofectamine 2000 (Invitrogen) and plasmids expressing BAP1-UCH, BAP1-ULD, and ASXL2-AB alone or in combination. At 48 hours post transfection, cells were collected, lysed, and whole cell lysates (WCL) were sonicated, followed by centrifugation for 20 min at 4°C max speed. Protein concentrations were measured by Bradford assay. For co-IP, 1 mg WCL were incubated in anti-FLAG M2 affinity gel (anti-Flag mAb, Sigma, cat. #A2220) and either anti-HA agarose beads (Thermo Scientific Pierce anti-HA agarose, cat. # 26181) or anti-Myc tag agarose beads (Thermo Scientific Pierce anti-c-Myc agarose; cat. #20169), which were prewashed with binding buffer. The binding buffer was composed of 50 mmol/L Tris-HCl, pH 7.4, 150 mmol/L NaCl, 2 mmol/L EDTA, 0.25% NP40, 2% BSA. IP was performed with rotation for 2 hours at 4°C. The resin then was then washed with buffer (50 mmol/L Tris-HCl, pH 7.4,150 mmol/L NaCl) 3 times, with 500 mmol/L NaCl used for the last wash, and then desalted with 20 mmol/L Tris-HCl, 5 mmol/L EDTA, 0.5%NP40 and extracted with 5x Laemmli sample buffer. The protein complex and 50 μg cell lysates were resolved in 4%−12% Bis-Tris NuPAGE gels (Invitrogen) in MOPS running buffer and transferred onto PVDF membranes (Millipore). WB analysis was performed as described, using the following antibodies: Myc-tag rabbit antibody (71D10; cat. #2278; 1:5,000), Myc-tag mouse antibody (9B11; cat. #2276; 1:10,000),Flag antibody (DYKDDDDK Tag, D6W5B; cat. #14793; 1:5000), and HA-tag antibody (C29F4; cat. #3724, 1:5000) (Cell Signaling Technology); GAPDH antibody (6C5, sc-32233, 1:50,000) (Santa Cruz Biotechnology); and anti-rabbit IgG, peroxidase-linked species-specific whole antibody (from donkey) secondary HRP-linked secondary antibody (cat. #NA 9341; 1:10,000) and anti-mouse IgG, peroxidase-linked species-specific whole antibody (from sheep) secondary antibody (cat. #NA 3911; 1:10,000) (GE Healthcare Life Sciences).

To purify protein complexes for subsequent Ub-AMC assays, 25 mg of whole lysates were incubated for 2 hours at 4°C with rotation with prewashed anti-FLAG M2 affinity gel (anti-Flag (mAb), Sigma; cat. #A2220) and anti-HA agarose beads (Thermo Scientific Pierce anti-HA agarose; cat. # 26181). After the incubation, the resins were washed 5 times with binding buffer, and the protein elution was performed under native conditions by competition with 3x Flag synthetic peptide (Pierce 3x DYKDDDDK peptide; cat. #A36805, 1.5 mg/ml), Myc-tag synthetic peptide (Pierce c-Myc peptide; cat. #20170, 0.5 mg/ml), or HA synthetic Peptide (Thermo Scientific; cat. #26184, 1mg/ml). Two rounds of elution were

performed; for each round, the samples was incubated with the elution peptide for 20 min at 37°C on a shaker table, and then the resin slurry was transferred to a spin column (Thermo Scientific Pierce spin columns; cat. # 69705) and spun down for 30 s to collect the elute. Resin was resuspended again in elution buffer, transferred to a new tube, incubated for another 20 min at 37°C on a shaker, and the elution repeated. WB was performed to check the elution of each protein. Ub-AMC assays were then performed. The eluted proteins in the complexes were detected and semi-quantified by WB. Progress curves monitoring the cleavage of Ub-AMC used dilutions of the co-IP elution samples that were chosen based upon densitometry analysis of the UCH band.

Results

Bap1 and Asxl protein co-expression in single cell RNAseq datasets

To build a cellular model of *Bap1* and *Asxl1–3* co-expression, we used the 53,760-cell dataset of 20 tissues from the mouse (26). *Bap1* expression was found to vary in the average counts per cell and the number of cells expressing the gene, with tissues such as thymus showing the highest *Bap1* levels (Supplementary Fig. S1A). Co-segregating gene expression in those cells expressing *Bap1* versus those that do not for the thymus revealed 122/289 genes that positively correlated to be involved in cell cycling (p-value, 3.5e-61) and several that were connected to BAP1 interaction pathways (Supplementary Fig. S1B). Interestingly, cancer-related genes such as *Fos* were negatively correlated with *Bap1*. Among the 20 tissues, the majority of *Bap1*-expressing cells had none of the *Asxl1–3* genes expressed (60.7%), with 21.1% of cells repressing *Asxl2*, 11.3% of cells with *Asxl1*, 5.9% of cells expressing both Asxl1 and Asxl2, and 0.9% with Asxl3 (Supplementary Fig. S1C), suggesting ASXL2 kinetic interactions are of the highest priority for ASXL proteins.

The breakdown of the 20 tissues showed a varying percentage of *Bap1* positive cells to have *Asxl1* or *Asxl2* expression, with tissues such as pancreas having the greatest *Asxl2* bias and those such as muscle having an *Asxl1* bias (Supplementary Fig. S1D). Correlation analysis of the single cells for each tissue revealed that liver and pancreas have higher correlations between *Asxl2* and *Bap1* expression levels (Supplementary Fig. S1E), with genes correlating to those *Bap1* and *Asxl2* positive-expressing cells having significantly enriched protein-protein interactions (PPI) and lipid metabolic process gene ontology (GO) for positively correlated genes and regulation of cell motility in negatively correlated genes (Supplementary Fig. S1F). We found that BAP1 and ASXL1/2 are highly expressed together within single-cell datasets for most organs, in which the cells show large transcriptional differences when the factors are co-expressed. This highlights the critical need to understand how the proteins synergistically regulate broad cell transcriptional processes.

Analysis of conserved and selected BAP1 and ASXL1–3 contact sites

The domain structure of BAP1 is unique from other UCH proteins (Fig. 1A). The N-terminus of BAP1 has similarity to other mammalian UCHs (UCHL1, UCHL3, and UCHL5); however, BAP1 also has several additional conserved motifs and domains throughout the remainder of the protein including the ULD found only in UCHL5. Alignments of the UCH domain of the four proteins and the ULD of BAP1 and UCHL5

identify many amino acids conserved throughout, especially at sites with cancer (COSMIC) mutations within the UCH (Fig. 1B, C). Using the structure of *Drosophila* Calypso UCH/ULD interaction with ASX (PDB 6HGC) converted into human BAP1 UCH/ULD and ASXL2 merged with our previous models of interaction with H2A and ubiquitin (16), we can pinpoint the human contact maps of the ULD with ASXL2 with high confidence (Fig. 1D, E). The BAP1 ULD contact amino acids have 12/22 amino acids fixed throughout the evolution of both BAP1 and UCH-L5, yet 7/22 amino acids are unique to BAP1 based on evolution, suggesting a possible altered interaction between ASXL2 and UCHL5 than with BAP1. Our observed conservation of ASXL1–3 with the *Drosophila* ASX protein identifies a shared highly conserved ASXH domain critical for ULD interaction as suggested by homology modeling of the PDB structure 6HGC of the *Drosophila* ASX and Calypso, where contact points are conserved between species and paralogs (Supplementary Fig. S2A). Of the BAP1 contact amino acids within ASXL2, 20/29 sites are conserved between *Drosophila* ASX and ASXL1–3 (Supplementary Fig. S2B). A total of 23/29 BAP1 contact sites are conserved throughout ASXL1–3, suggesting that contact between ASXL1–3 with BAP1 are maintained throughout all three proteins.

Of note, the BAP1-UCH loop is larger than the ones in other UCH proteins, with a high conservation of both these loop amino acids and of multiple amino acids structurally near this loop (Fig. 1B, D, E), implying that larger substrates may be available to BAP1's catalytic cleavage site than for other UCH domains, yielding a BAP1-specific recruitment of proteins/domains such as ASX and ULD for enzyme regulation (21). ASXL behaves as a scaffold that recruits BAP1 to transcription factors that bind to target genes (17). Subsequently, the BAP1 ubiquitin hydrolase removes ubiquitin from histones on chromatin to regulate the activity of these target genes. ASXL also greatly stimulates BAP1 activity. When genetic alterations occur in *BAP1*, they result in enzymatic loss-of-function of BAP1 or abolish BAP1's interaction with ASXL. Loss of binding to ASXL would dramatically decrease BAP1 deubiquitination activity, because of an inability to bring ASXL to BAP1's catalytic site. On the other hand, products of *ASXL* gene mutations that lose association with BAP1 also lead to BAP1 loss of function (16). The structure of the BAP/ASXL2 tripartite complex has not been determined; however, the crystal structure of the *Drosophila* Calypso and its activating partner ASX was recently determined (21). The stoichiometry of BAP and ASXL1–3 interaction and the kinetics remained unknown. Therefore, we initiated biochemical and biophysical analyses of the BAP1-UCH, BAP1-ULD, ASXL2-AB domains and protein complex.

Purification of recombinant proteins and protein complex

His- or GST-tagged full-length BAP1, BAP1-UCH and BAP1-ULD domains were expressed in bacteria (Bac-) or baculovirus (Bv-), respectively (Supplementary Fig. S3A). The reasons that we expressed the proteins in baculovirus were in case post-translational modifications are needed for the protein functions and/or that other cellular factors are involved in the protein functions. All the baculovirus-expressed proteins and domains were soluble using Ni^{2+}-NTA chromatography under native purification conditions (Supplementary Fig. S3B) and the proteins were functional (see below). The bacterial-expressed GST-BAP1-UCH and GST-BAP1-ULD were soluble using GST-chromatography under native purification

conditions (Supplementary Fig. S3B) and the proteins were functional (see below). The bacterial-expressed His-BAP1-ULD and His-ASXL2-AB proteins were purified under denaturing conditions, followed by a re-naturation protocol that yielded soluble, highly active proteins (Supplementary Fig. S3B). However, the yield of re-folded proteins was not sufficient for structural studies. We thus used the pETDuet co-expression system to co-express His-ULD and AB, or His-AB and ULD protein complexes in *E. coli* (Rosetta 2 (DE3) pLysS)]. The His-ULD/AB protein complex was successfully co-expressed and then purified using cobalt beads (Talon) under native purification conditions. The protein complex was highly soluble and functional.

Biophysical and biochemical characterization of BAP1-UCH, BAP1-ULD, ASXL2-AB, and the UCH/ULD/AB complex

To evaluate the behavior of individual proteins and their complexes, we examined mono-dispersion of His-ULD, His-AB and His-ULD/AB complexes using DLS. We tested a full spectrum of buffer conditions for optimizing the solubility and stability of individual proteins and protein complexes. Under the optimal buffer condition found (50 mM potassium phosphate, pH 7.5, 200 mM potassium chloride and 1 mM TCEP), His-AB and His-ULD were mono-dispersed 87% and 88%, respectively (Fig. 2A). However, when the ULD-AB complex is formed, the mono-dispersion was 91.8%, indicating a similar, or perhaps slightly higher stability of the complex than for the individual proteins. In addition, we observed a shift in the scan to a smaller size complex when these protein domains were bound together. Thus, it appears that the complex is more tightly packed spatially than the individual proteins. This result is consistent with the CD data presented, which showed additional secondary structure formation attained during binding. In addition, these proteins were utilized for further ITC experiments (Fig. 2B) in calculating concentrations used, because it is assumed only the mono-dispersed species is capable of interacting properly with the other complex members.

Since the binding kinetics and stoichiometry of interaction of the ULD domain and the AB box have remained unknown until now, we next decided to determine the thermodynamics, kinetics, and stoichiometry of this domain-domain interaction using ITC technology. Highly purified His-ULD and His-AB proteins were critically equilibrated in the same buffer (50 mM potassium phosphate, pH 7.5, 200 mM potassium chloride and 1 mM TCEP). The His-AB was placed in the ITC cell with 77 μM protein concentration while the titrated protein His-ULD was at 574 μM protein concentration. We also set the references for each protein (see Materials and Methods) for subtraction from the experimental data. The data showed that K_d for interaction of His-ULD and His-AB is approximately 4.26 μM (3.73 μM-4.85 μM). The stoichiometry of His-ULD to His-AB is 1:1 molar ratio (Fig. 2B). We also observed that the thermodynamics of the interaction has a ΔH of −9.87 kcal/mol and ΔS of −10.3 cal/mol/deg, indicating an exothermic interaction. These data are consistent with our previous studies that used computer modeling technology to predict the molecular model of BAP1-ULD interacting with ASXL2-AB (16). The interaction for both ULD and AB has a modest binding affinity dissociation constant, a result consistent with expectations of formation of a protein-protein complex in a reversible manner.

From our previous computer modeling studies, BAP1-ULD is predicted to form a few long helices, while ASXL-AB box is predicted to form five helices (16). We have now performed CD to determine the secondary structure of the purified recombinant protein His-ULD, His-AB and His-ULD/AB complex. The CD spectra of the domains and complex demonstrated that each of these proteins and the protein complex adopts a partially helical conformation and has a high degree of secondary structure (Fig. 2C). While His-AB appears to be partly unstructured as demonstrated by a broad minima at 208 nm, this minima is lessened in the His-ULD/AB complex. The complex also has increased alpha-helical content relative to the two monomer proteins as indicated by an increased minima at 222 nm.

Biochemical analyses of purified recombinant protein complexes from bacteria reveal a direct interaction between the BAP1-ULD domain and ASXL2-AB box

Using computer molecular modeling of UCHL5 structures, we predicted that the BAP1-ULD domain folds back to the BAP1-UCH catalytic domain and that the ASXL2-AB box stabilizes the UCH catalytic loop via a unique BAP1 mechanism not seen in other UCH proteins, allowing for ubiquitin to fit into the active site (Fig. 1D, E). We previously demonstrated that the GST-UCH directly interacts with the ULD domain but does not directly interact with the AB box, whereas the ULD domain recruits the AB box to form a stable complex (16). In our new work, we co-expressed and co-purified the His-ULD/AB domain complex using the pETDuet system, which allowed us to obtain a well-folded protein complex (Supplementary Fig. S3B). To test this highly purified protein complex, a GST association assay was performed. GST or GST-UCH was pre-coated on the GST resin, followed by incubation with His-ULD/AB complex. After washing with BB200 or BB500 buffer, the GST resin with protein complex was extracted, analyzed by SDS-PAGE, and stained with Coomassie blue. The result demonstrated that the His-ULD/AB complex was pulled down by GST-UCH but not by GST (Fig. 2D). The UCH/ULD/AB protein complex was indeed formed.

Biochemical analyses of purified recombinant protein complexes demonstrate stimulation of BAP1 deubiquitinase activity by ASXL2-AB and ULD/AB

We then used the fluorogenic substrate Ubiquitin-AMC (Ub-AMC) to measure BAP1 deubiquitinase activity. The activity of the UCH domain of BAP1 was ~5-fold greater than the full-length BAP1, with specific activity values of 358 ± 6.6 pmol AMC/min/pmol E and 73 ± 2.4 pmol AMC/min/pmol E, respectively (Fig. 3A). For both full-length BAP1 and the UCH domain, a point mutation of the cysteine residue at position 91 completely abolished enzyme activity (Fig. 3A), consistent with previous observations (16).

We further characterized the stimulating effect of the ASXL-AB box on BAP activity by testing increasing concentrations of the AB box in the presence of a substrate titration of Ub-AMC. ASXL2-AB dose-dependently increased the maximal velocity (V_{max}) of BAP1 cleavage of Ub-AMC by 2.5-fold (Fig. 3B). The K_m values for Ub-AMC in the presence of increasing concentrations of ASXL2-AB ranged from 4–9 mM and did not correlate with ASXL2-AB concentration, suggesting that the ASXL2-AB box stimulates BAP1 enzyme activity by increasing its V_{max}, rather than the K_m for Ub-AMC. We also were able to obtain a functional potency for ASXL2-AB stimulation of BAP1 enzyme activity by plotting the

V_{max} values for BAP1 enzyme activity against the concentration of ASXL2-AB box. These data fit well to a typical one-site dose response curve with a Hill slope of 1.0 and an EC_{50} of 0.96 nM (95%CI: 0.42–2.4 nM) (Fig. 3B).

We then determined the functional potency of co-expressed/co-purified His-ULD/AB complex. Since we established that ASXL2-AB stimulates BAP1 deubiquitinase activity by increasing the V_{max}, we measured the specific activity of BAP1 in the presence of increasing concentrations of His-ULD/AB in order to conserve substrate (Fig. 3C). The His-ULD/AB complex stimulated BAP1 specific activity 4.5 fold using 100 nM Ub-AMC. Data-plotting the specific activity values against ULD/AB concentration fit well to a one-site dose response curve with a Hill slope of 1.0 and an EC_{50} of 2.8 nM (95%CI: 1.0–7.5 nM) (Fig. 3C), which is within 3 fold of the functional potency we obtained for ASXL2-AB.

Kinetic studies of the interactions between AB and ULD domains, ULD/AB complex and full-length BAP and BAP-UCH

We next tested the affinity and kinetics of BAP1-ULD and ASXL2-AB using SPR. ASXL2 was found to bind to GST-ULD, but not GST-UCH or GST alone (Fig. 4A). ASXL2 bound with moderate affinity to GST-ULD, with a steady state K_D value of 134 nM (95% CI: 120–149 nM), (Fig. 4B, C, D). The kinetics of the interaction was relatively fast, with an association rate of $3.8 \times 10^4\ M^{-1}\ s^{-1}$ and a dissociation rate of $2.4 \times 10^{-3}\ s^{-1}$ (Fig. 4D). The K_D of 67 nM determined by these kinetic parameters was in good agreement with the K_D obtained from steady-state analysis.

ASXL2-AB by itself did not bind to the UCH domain of BAP1 as determined by SPR (Fig. 4A). Our hypothesis is that both the UCH and ULD domains of BAP1 interact with ASXL2-AB to stabilize the catalytic loop of the UCH domain. Therefore, we investigated the binding of the ULD/AB complex to both the UCH domain and full-length BAP1 using SPR. We found that the ULD/AB complex binds to both full-length BAP1 and GST-UCH with relatively low affinity, but it did not bind GST alone (Fig. 5A). The steady-state K_D values for full-length BAP1 and GST-UCH were 1910 nM (95% CI: 1600–2400 nM) and 740 nM (95% CI: 580–950), respectively (Fig. 5D). The kinetics of the interaction between the ULD/AB complex and either full-length BAP1 (Fig. 5C) or GST-UCH (Fig. 5B) were characterized by fast association and dissociation rates. The association rates of ULD/AB binding were $3.9 \times 10^4\ M^{-1}\ s^{-1}$ and $1.9 \times 10^4\ M^{-1}\ s^{-1}$ for full-length BAP1 and GST-UCH, respectively, and the dissociation rates were $0.033\ s^{-1}$ and $0.044\ s^{-1}$, respectively (Fig. 5B, C, D). The K_D values of 850 nM and 2300 nM for BAP1 and GST-UCH, respectively, that were obtained from these kinetic parameters, were in good agreement with those calculated from steady state analysis (Fig. 5B, C, D).

In vitro validation of the interaction/regulation between ASXL and BAP1

To validate interactions between the ASXL2 and BAP1 and to show that the ASXL2-AB box can regulate BAP1 deubiquitinase activity in cells, we performed co-IP-WB assays on purified proteins from transfected HEK 293 cells. HEK-293 cells were co-transfected or triple transfected with different combinations of Myc-tag UCH and Myc-tag ULD domains of BAP1 and the Flag-tag ASXL2-AB box. The co-IP assays demonstrated that the UCH

domain of BAP1 alone does not bind to the ASXL2-AB box. Instead, the BAP1 ULD domain binds to the AB box, which leads to the formation of a stable ternary complex consisting of the BAP1-UCH, BAP1-ULD and ASXL2-AB domains (Figure 6A–D). These data are consistent with our biochemical data.

Stimulation of BAP1 deubiquitinase activity in cells by ASXL2-AB and ULD/AB complexes

In addition, to measure the amount of stimulation of BAP deubiquitinase activity by the ASXL-AB domain, we performed Ub-AMC assays on purified protein from human cells expressing exogenous ASXL-AB, BAP-UCH, and/or BAP-ULD domains and purified protein complexes (Fig. 7A, B). The experiments revealed that a purified AB-ULD-UCH protein complex exhibited the highest Ub-AMC activity (Fig. 7C, D), confirming our biochemical findings.

Discussion

Our previous biochemical studies showed that the ASXL2-AB box is the minimal domain required to interact with and stimulate the deubiquitinase activity of BAP1 (16). Mutations in the AB box or in the ULD domain of BAP1 either partially or completely impacted the AB and ULD interaction and UCH ubiquitin hydrolase activity (16). Deletion of R666-H669 in the ULD domain of BAP1, corresponding to alterations observed in some human uveal melanomas and malignant mesotheliomas, completely abolished binding to the AB box.

In the present study, we quantified the stimulatory effect of the AB box on both full-length BAP1 and UCH domain deubiquitinase activity. Based on the molecular dynamics, kinetics, and stoichiometry of the intra- and inter-molecule domain-domain interactions between BAP1 and ASXL2 presented here, we draw the following conclusions. First, all of the single- or co-expressed and purified recombinant BAP1 and ASXL2 domain/proteins or protein complexes from both bacteria and baculovirus are well-folded in structure and are functionally active. Second, the interaction between BAP1 and ASXL2 is direct, specific, and stable to biochemical and biophysical manipulations. The association of the AB box greatly stimulates BAP1 deubiquitinase activity, and this interaction does not require post-translational modifications. A stable ternary complex was formed in UCH/ULD/AB domains. Third, the binding affinity of the ULD domain of BAP to the AB box of ASXL2 is very high, with fast association and slow dissociation rates. One molecule of the ULD domain directly interacts with one molecule of the AB box. Fourth, the formation of this ULD/AB complex with the UCH domain is a single-step event with fast association and slow dissociation rates, indicating that this interaction occurs very rapidly.

Importantly, the high quality of the bacterial- and baculoviral-expressed proteins and protein complexes were highly functional, which allowed us to study the dynamic kinetics of their interactions and the stoichiometry of the protein complex association by ITC and SPR and to perform highly sensitive assays to evaluate deubiquitinase-specific activity of BAP1 and the direct effects of stimulation of ASXL2 on BAP1 enzymatic activity. We found that these domain-domain interactions and ternary complex interactions were direct and stable and do not require post-translational modifications. This is quite different from other protein-protein interactions that require post-translational modifications (27). We not only were able to

reconstitute the tripartite domain complex *in vitro*, but we were also able to study the real-time dynamic kinetics of domain-domain and tripartite domain interactions. SPR technology has been established for studying real-time dynamic kinetics of DNA-protein and protein-protein interactions (23,28), and this methodology permitted us to determine that the binding mode either for AB on ULD or ULD/AB on UCH occurs by a single-step event with fast association and slow dissociation rates, indicating these interactions are very rapid. Moreover, the stoichiometry of AB and ULD association occurs via one molecule of AB binding to one molecule of ULD with high affinity, which is consistent with the crystal structure of *Drosophila* Calypso/ASX, which has a stoichiometry of 1:1 molar ratio at low protein concentrations, and 2:2 molar ratio at high protein concentrations (21).

Our new findings are consistent with our molecular modeling data suggesting that the AB box does not induce a conformational change in the substrate's binding pocket, but instead binds to the ULD domain and stabilizes the UCH loop of BAP1. The potency of the AB box for stimulating BAP1 mediated cleavage of Ub-AMC is similar to the concentration of BAP1 in the enzyme assay, which suggests a 1:1 interaction. This is consistent with the ITC results reported here. The establishment of Ub-AMC assay and SPR for investigating protein-protein interactions would make it possible to validate small molecule hits in future screens for drug compounds that recover loss-of-function in cells with BAP1-ULD mutations/deletions (29).

Interestingly, the ULD/AB complex, but not the AB box alone, was able to bind the BAP1-UCH domain, as determined by SPR, suggesting that interaction with the ULD domain is essential for stabilizing the UCH domain of BAP1. As the ULD is also found in UCHL5, this makes sense. In addition, most of the affinity for the AB box for BAP1 is through the ULD domain, as this interaction had 10- to 20-fold higher affinity compared to the affinity of the ULD/AB complex for the UCH domain. These data suggest that the AB box binds the ULD domain first, and this complex then interacts with the BAP1-UCH domain to stimulate enzyme activity.

This investigation represents the first quantitative assessment of the inter- and intra-molecular interactions of the BAP1 tumor suppressor and its obligate partner for enzymatic activity, ASXL2, including the mode by which the ASXL2-AB box mediates BAP1 deubiquitinase activity. The tripartite (UCH/ULD/AB) domain-domain interactions described here explain the loss of the BAP1 deubiquitinase activity when tumor-associated mutations in *BAP1* occur outside of the catalytic UCH domain, each failing to productively recruit the AB box to the wild-type BAP1 catalytic site via the ULD, resulting in loss of BAP1 deubiquitinase activity.

Recently, two groups have reported the crystal structure of the BAP1 ortholog, Calypso, bound to its activating partner, ASX, the homolog of ASXL (21,30). This structural work has helped elucidate the molecular mechanism by which Calypso/BAP1 activation by ASX/ASXL mediates gene repression by cleaving ubiquitin from histone H2A in nucleosomes. Moreover, Ub-AMC enzymatic assays revealed that Calypso cleaves ubiquitin from Ub-AMC and retains DUB activity toward ubiquitinated nucleosomes (30). Similar to our findings, these studies provided molecular insights into BAP1 function and its regulation by

ASXL, as well as demonstrating that cancer-related mutations of BAP1 and ASXL1 affect BAP1 activation by ASXL and Ub binding. Our data are also consistent with those of Daou et al. (31), who showed that interaction between the DEUBiquitinase ADaptor (DEUBAD) domain (dubbed AB box in our study) of ASXL and the C-terminal domain (CTD) (referred to as ULD domain in our study) of BAP1 are prerequisite for the assembly of the DUB competent complex. Monoubiquitination of the DEUBAD (AB box) stabilizes ASXL2, stimulates ubiquitin binding and BAP1 DUB activity and regulates mammalian cell proliferation, similar to what we have reported in our earlier biochemical studies (16). Moreover, the protein levels of BAP1, ASXL2, and UBE2E enzymes have been reported to be highly correlated in human malignant mesotheliomas, suggesting that this signaling axis plays an important role in tumor suppression (31).

In conclusion, by the combined use of biochemistry, biophysics and *in vitro* studies, we have provided evidence supporting the molecular mechanism by which ASXL mediates BAP1 deubiquitinase activity. We have demonstrated that ASXL, via its AB box, acts as a molecular scaffold to recruit the BAP1-ULD domain to transcription factors that bind to specific target genes; the BAP1-UCH catalytic domain then removes ubiquitin from histones on chromatin to regulate the expression of these transcriptional targets (Supplementary Fig. 4). Thus, ASXL behaves as both a molecular scaffold for BAP1 and stimulates its deubiquitinase activity. Upon loss of binding of the ASXL-AB box to BAP1-ULD, BAP1 enzymatic activity is abolished, resulting in disturbances in BAP1-dependent chromatin state/gene expression that contribute to the pathogenesis of human malignancy and other diseases. Small-molecule approaches to reactivate latent wild-type UCH activity of these mutants occurring in a subset of BAP1-mutant cancers might be therapeutically viable.

Supplementary Material

Refer to Web version on PubMed Central for supplementary material.

Acknowledgments

We thank Katherine L.B. Borden and Michael Osborne (University of Montreal) for their advice and suggestions related to this project and manuscript. This work was supported by NCI grants R01CA175691 (J.R. Testa, F.J. Rauscher), P30CA006927 (Fox Chase Cancer Center), P30CA010815 (F.J. Rauscher), R01CA163761 (F.J. Rauscher), and NIH Office of the Director grant K01ES025435 (J.W. Prokop). Support for Shared Resources was provided by P30CA010815 to The Wistar Institute. Also supported by the Jayne Koskinas Ted Giovanis Foundation for Health and Policy (F.J. Rauscher), the Palmira and James Nicolo Family Research Fund (S.B. Malkowicz), Local #14 Mesothelioma Fund of the International Association of Heat and Frost Insulators and Allied Workers (J.R. Testa), Samuel Waxman Cancer Research Foundation (F.J. Rauscher), and Office of the Assistant Secretary of Defense for Health Affairs, through the Breast Cancer Research Program, under Award numbers W81XWH-17-1-0506, W81XWH-14-1-0235 and W81XWH-11-1-0494 (F.J. Rauscher). This work was also supported by grants 1K22A154600 and 1R03A188439 (E.J. Kennedy).

The abbreviations used are:

UCH	ubiquitin C-terminal hydrolase
ULD	UCH37-like domain
PcG	polycomb group (PcG)

PR-DUB	polycomb repressive deubiquitinase
ASXH	ASX homology domain
PHD	plant homeo domain
PRC2	polycomb repressive complex 2
NLS	nuclear localization signals
Bac	bacteria
Bv	baculovirus
SPR	surface plasmon resonance
ITC	isothermal titration calorimetry
CD	circular dichroism
DLS	dynamic light scattering

References

1. Jensen DE, Proctor M, Marquis ST, Gardner HP, Ha SI, Chodosh LA, et al. BAP1: a novel ubiquitin hydrolase which binds to the BRCA1 RING finger and enhances BRCA1-mediated cell growth suppression. Oncogene 1998;16:1097–112. [PubMed: 9528852]
2. Nishikawa H, Wu W, Koike A, Kojima R, Gomi H, Fukuda M, et al. BRCA1-associated protein 1 interferes with BRCA1/BARD1 RING heterodimer activity. Cancer Res 2009;69:111–9. [PubMed: 19117993]
3. Misaghi S, Ottosen S, Izrael-Tomasevic A, Arnott D, Lamkanfi M, Lee J, et al. Association of C-terminal ubiquitin hydrolase BRCA1-associated protein 1 with cell cycle regulator host cell factor 1. Mol Cell Biol 2009;29:2181–92. [PubMed: 19188440]
4. Gaytan de Ayala Alonso A, Gutierrez L, Fritsch C, Papp B, Beuchle D, Muller J. A genetic screen identifies novel polycomb group genes in *Drosophila*. Genetics 2007;176:2099–108. [PubMed: 17717194]
5. Scheuermann JC, de Ayala Alonso AG, Oktaba K, Ly-Hartig N, McGinty RK, Fraterman S, et al. Histone H2A deubiquitinase activity of the Polycomb repressive complex PR-DUB. Nature 2010;465:243–7. [PubMed: 20436459]
6. Inobe T, Matouschek A. Paradigms of protein degradation by the proteasome. Curr Opin Struct Biol 2014;24:156–64. [PubMed: 24632559]
7. Isaksson A, Musti AM, Bohmann D. Ubiquitin in signal transduction and cell transformation. Biochim Biophys Acta 1996;1288:F21–9. [PubMed: 8764838]
8. Kadariya Y, Cheung M, Xu J, Pei J, Sementino E, Menges CW, et al. Bap1 is a bona fide tumor suppressor: genetic evidence from mouse models carrying heterozygous germline *Bap1* mutations. Cancer Res 2016;76:2836–44. [PubMed: 26896281]
9. Bott M, Brevet M, Taylor BS, Shimizu S, Ito T, Wang L, et al. The nuclear deubiquitinase BAP1 is commonly inactivated by somatic mutations and 3p21.1 losses in malignant pleural mesothelioma. Nat Genet 2011;43:668–72. [PubMed: 21642991]
10. Harbour JW, Onken MD, Roberson ED, Duan S, Cao L, Worley LA, et al. Frequent mutation of *BAP1* in metastasizing uveal melanomas. Science 2010;330:1410–3. [PubMed: 21051595]
11. Testa JR, Cheung M, Pei J, Below JE, Tan Y, Sementino E, et al. Germline *BAP1* mutations predispose to malignant mesothelioma. Nat Genet 2011;43:1022–5. [PubMed: 21874000]

12. Abdel-Rahman MH, Pilarski R, Cebulla CM, Massengill JB, Christopher BN, Boru G, et al. Germline *BAP1* mutation predisposes to uveal melanoma, lung adenocarcinoma, meningioma, and other cancers. J Med Genet 2011;48:856–9. [PubMed: 21941004]
13. Carbone M, Yang H, Pass HI, Krausz T, Testa JR, Gaudino G. BAP1 and cancer. Nat Rev Cancer 2013;13:153–9. [PubMed: 23550303]
14. Pilarski R, Rai K, Cebulla C, Abdel-Rahman M. BAP1 Tumor Predisposition Syndrome. In: Adam MP, Ardinger HH, Pagon RA, Wallace SE, Bean LJH, Stephens K, et al., editors. Seattle, WA: GeneReviews®; 2016.
15. Wiesner T, Obenauf AC, Murali R, Fried I, Griewank KG, Ulz P, et al. Germline mutations in *BAP1* predispose to melanocytic tumors. Nat Genet 2011;43:1018–21. [PubMed: 21874003]
16. Peng H, Prokop J, Karar J, Park K, Cao L, Harbour JW, et al. Familial and somatic *BAP1* mutations inactivate ASXL1/2-mediated allosteric regulation of BAP1 deubiquitinase by targeting multiple independent domains. Cancer Res 2018;78:1200–13. [PubMed: 29284740]
17. Abdel-Wahab O, Adli M, LaFave LM, Gao J, Hricik T, Shih AH, et al. *ASXL1* mutations promote myeloid transformation through loss of PRC2-mediated gene repression. Cancer Cell 2012;22:180–93. [PubMed: 22897849]
18. Bainbridge MN, Hu H, Muzny DM, Musante L, Lupski JR, Graham BH, et al. De novo truncating mutations in *ASXL3* are associated with a novel clinical phenotype with similarities to Bohring-Opitz syndrome. Genome Med 2013;5:11. [PubMed: 23383720]
19. Hoischen A, van Bon BW, Rodriguez-Santiago B, Gilissen C, Vissers LE, de Vries P, et al. De novo nonsense mutations in *ASXL1* cause Bohring-Opitz syndrome. Nat Genet 2011;43:729–31. [PubMed: 21706002]
20. Argote A, Mora-Hernandez O, Milena Aponte L, Barrera-Chaparro DI, Munoz-Ruiz LM, Giraldo-Mordecay L, et al. Cardiovascular risk factors and carotid intima-media thickness in a Colombian population with psoriasis. Actas Dermosifiliogr 2017;108:738–45. [PubMed: 28662815]
21. Foglizzo M, Middleton AJ, Burgess AE, Crowther JM, Dobson RCJ, Murphy JM, et al. A bidentate Polycomb Repressive-Deubiquitinase complex is required for efficient activity on nucleosomes. Nat Commun 2018;9:3932. [PubMed: 30258054]
22. Peng H, Begg GE, Schultz DC, Friedman JR, Jensen DE, Speicher DW, et al. Reconstitution of the KRAB-KAP-1 repressor complex: a model system for defining the molecular anatomy of RING-B box-coiled-coil domain-mediated protein-protein interactions. J Mol Biol 2000;295:1139–62. [PubMed: 10653693]
23. Peng H, Begg GE, Harper SL, Friedman JR, Speicher DW, Rauscher FJ 3rd. Biochemical analysis of the Kruppel-associated box (KRAB) transcriptional repression domain. J Biol Chem 2000;275:18000–10. [PubMed: 10748030]
24. Prokop JW, Lazar J, Crapitto G, Smith DC, Worthey EA, Jacob HJ. Molecular modeling in the age of clinical genomics, the enterprise of the next generation. J Mol Model 2017;23:75. [PubMed: 28204942]
25. Forbes SA, Beare D, Gunasekaran P, Leung K, Bindal N, Boutselakis H, et al. COSMIC: exploring the world's knowledge of somatic mutations in human cancer. Nucleic Acids Res 2015;43:D805–11. [PubMed: 25355519]
26. Consortium TM. Single-cell transcriptomics of 20 mouse organs creates a Tabula Muris. Nature 2018;562:367–72. [PubMed: 30283141]
27. Ivanov AV, Peng H, Yurchenko V, Yap KL, Negorev DG, Schultz DC, et al. PHD domain-mediated E3 ligase activity directs intramolecular sumoylation of an adjacent bromodomain required for gene silencing. Mol Cell 2007;28:823–37. [PubMed: 18082607]
28. Chang AT, Liu Y, Ayyanathan K, Benner C, Jiang Y, Prokop JW, et al. An evolutionarily conserved DNA architecture determines target specificity of the TWIST family bHLH transcription factors. Genes Dev 2015;29:603–16. [PubMed: 25762439]
29. Kortagere S, Mortensen OV, Xia J, Lester W, Fang Y, Srikanth Y, et al. Identification of novel allosteric modulators of glutamate transporter EAAT2. ACS Chem Neurosci 2018;9:522–34. [PubMed: 29140675]

30. De I, Chittock EC, Grotsch H, Miller TCR, McCarthy AA, Muller CW. Structural basis for the activation of the deubiquitinase Calypso by the Polycomb protein ASX. Structure 2019;27:528–36 e4. [PubMed: 30639226]

31. Daou S, Barbour H, Ahmed O, Masclef L, Baril C, Sen Nkwe N, et al. Monoubiquitination of ASXLs controls the deubiquitinase activity of the tumor suppressor BAP1. Nat Commun 2018;9:4385. [PubMed: 30349006]

Implications:

Collectively, these data elucidate molecular interactions between specific protein domains regulating BAP1 deubiquitinase activity, thus establishing a foundation for small-molecule approaches to reactivate latent wild-type BAP1 catalytic activity in *BAP1*-mutant cancers.

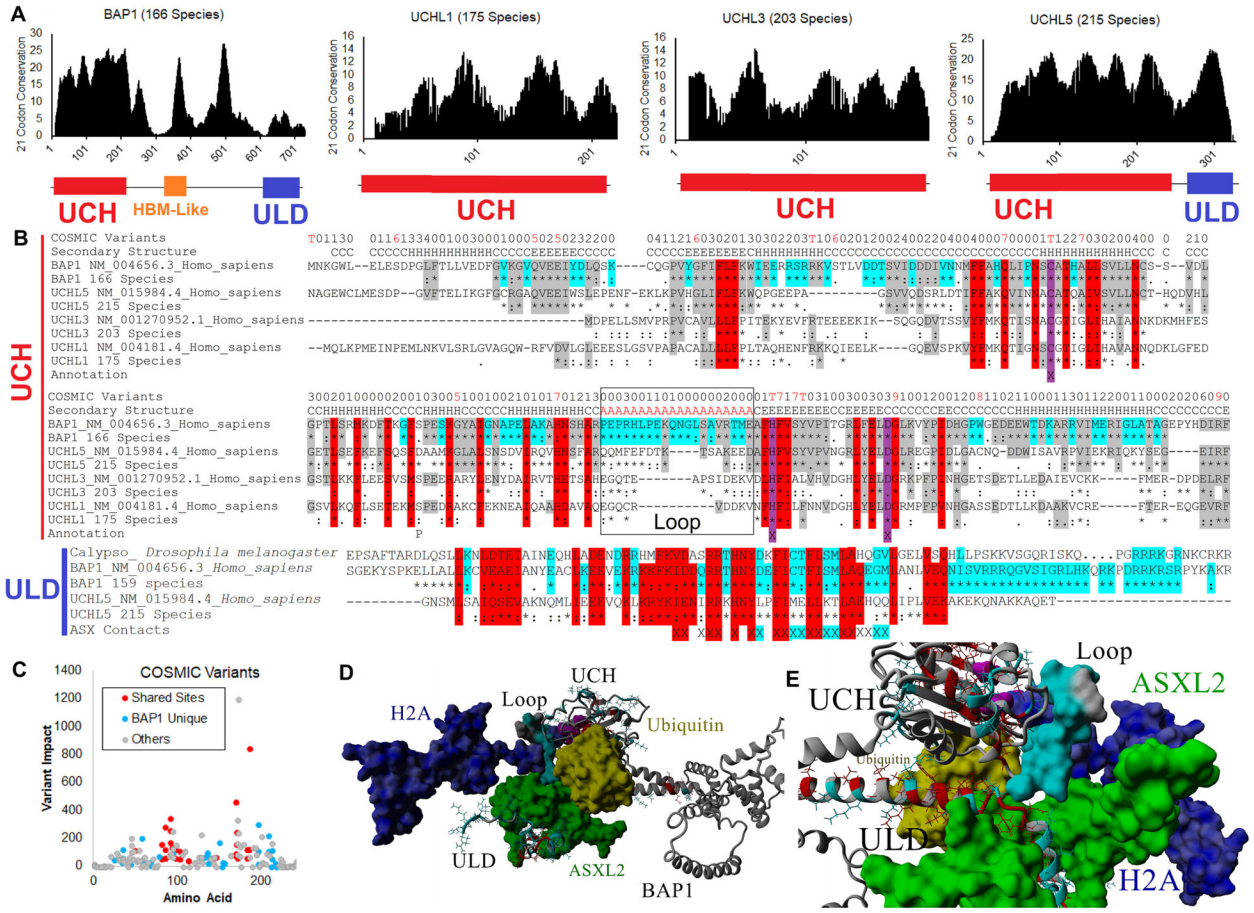

Figure 1.

BAP1 structure and evolution. **A,** Open reading frame sequences were aligned for each UCH protein followed by assessment of amino acid conservation and codon selection. Number of each species' sequences used is listed next to each name. The scores for each site are placed on a 21-codon sliding window, adding scores for 10 up- and down-stream of any site. Annotated domains are shown below each. **B,** Sequence alignments of UCH domain (red line) or ULD (blue line) of BAP1, UCHL5, UCHL3, and UCHL1 showing the human sequence and the consensus alignment information below each (***** = conserved in all species for each gene; : = functionally conserved for each gene; . = weakly conserved in each gene). Shown on the top is the number of COSMIC variants observed at each site (T = values ≥10), and below that is the secondary structure annotated based on protein modeling of the UCH. The X in annotation marks amino acids in the enzyme active site. Amino acids highlighted in red are conserved in all sequences, those in gray are conserved in at least two different proteins, and those in cyan are conserved and unique to BAP1. Sequence alignment of the ULD of BAP1 and UCHL5 includes the *Drosophila* Calypso sequence and the ASX contact amino acids marked with X. **C,** COSMIC variants of the UCH annotated for variant impact and based on conservation with other UCH proteins with coloring based on panel B. **D-E,** Model of the BAP1-UCH domain with colors shown from the previous alignments with additional bound H2A (blue) with ubiquitin (yellow), and the ULD (conservation based on alignment in panel B) revealing additional BAP1 uniquely conserved amino acids for the

stabilization by ASXL2 depicted in green near the UCH loop (cyan). The entire complex is shown in panel D, and a magnified view of the ASXL2, ULD, and UCH interaction is depicted in panel E.

A

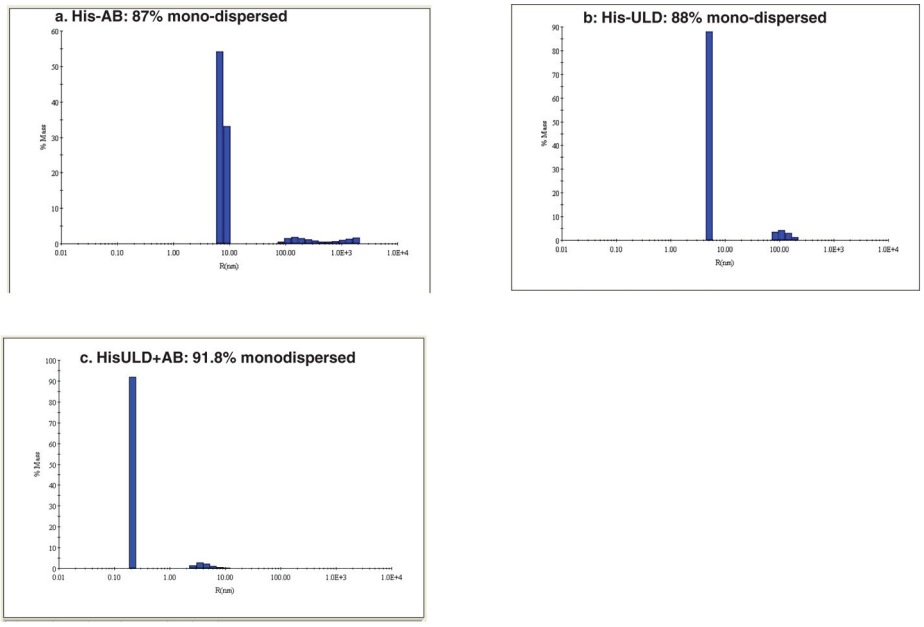

B

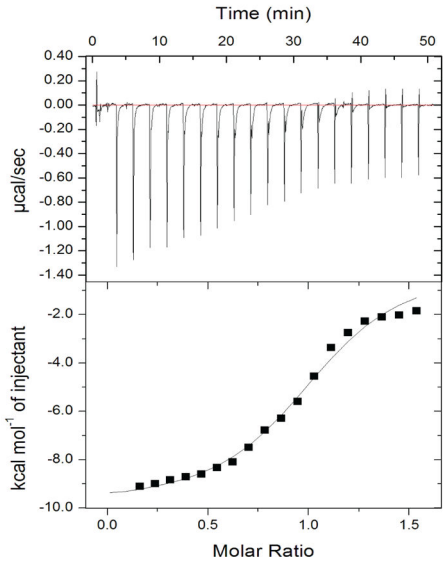

Interaction between BAP-ULD and ASXL2-AB	
Chi^2/DOF	6.71×10^4
Stochiometry (N)	1:1.03 ± 0.0138
K_A (M^{-1})	$2.35 \times 10^5 \pm 3.12 \times 10^4$
K_D (M)	4.26×10^{-6}
ΔH (cal/mol)	-9870 ± 205
ΔS (cal/mol/deg)	-10.3

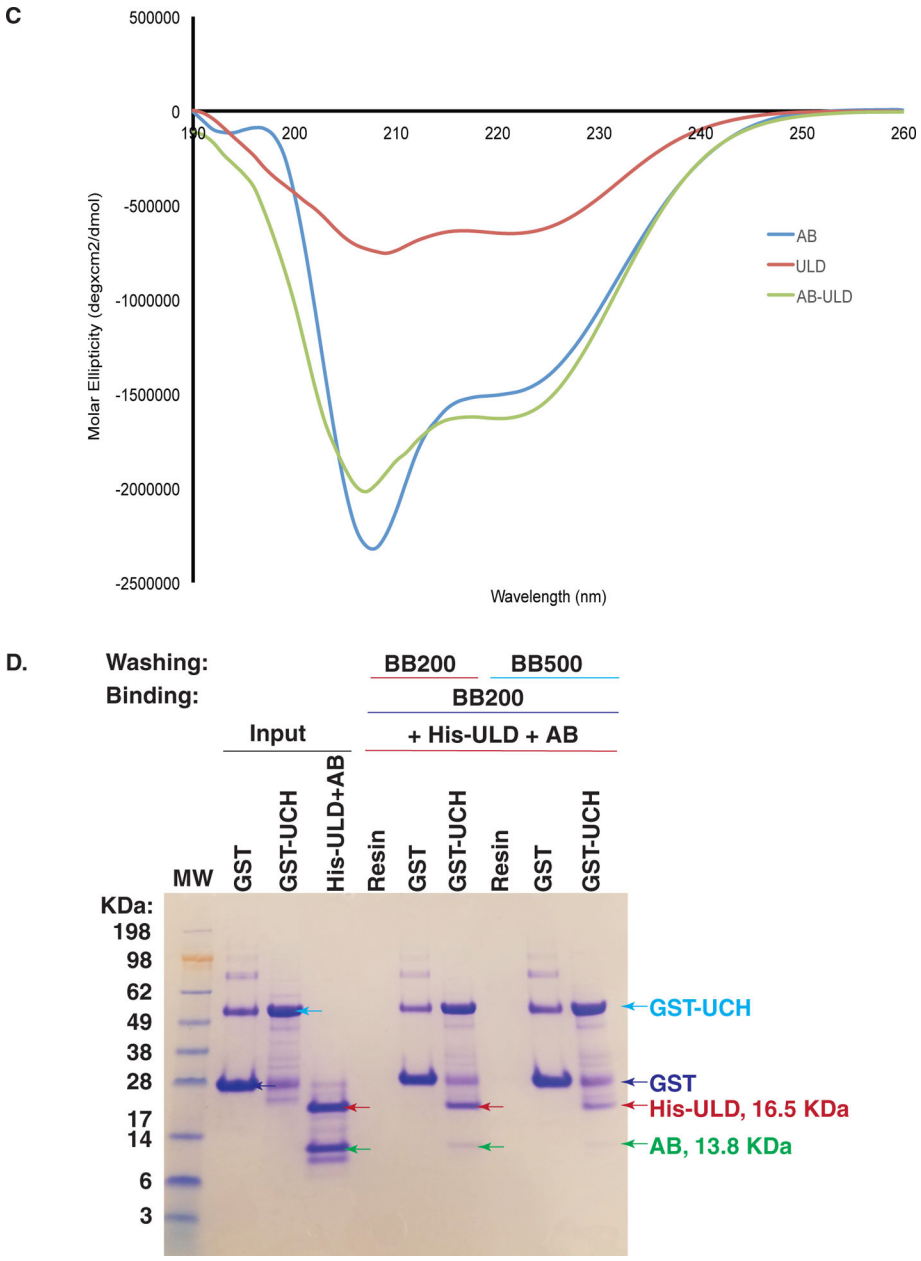

Figure 2.

Biochemical and biophysical analyses of purified proteins and protein complex from BAP1 and ASXL2. **A,** Dynamic light scattering (DLS) was used to examine the mono-dispersion of His-AB, His-ULD, and His-ULD/AB complex. Under the optimal buffer condition, His-AB and His-ULD proteins showed 87% and 88% mono-dispersion, respectively, whereas His-ULD/AB protein complex exhibited a higher degree (91.8%) of mono-dispersion, as directly measured by DLS. **B,** Isothermal titration calorimetry (ITC) was used to determine the thermodynamics and kinetics of domain-domain interactions between His-ULD and His-AB and their stoichiometry. 574 μM His-ULD protein was titrated into 77 μM His-AB protein in terms of molar ratio. ITC calculations derived from the direct measurements and curve fitting were performed using Origin 7 software. The binding affinity with dissociation

constant of the protein-protein interaction and the stoichiometry of the protein complex were determined. **C,** Circular dichroism was performed to determine the secondary structure of purified His-ULD and His-AB proteins as well as the His-ULD/AB protein complex. Data were processed using the Jasco Spectra Manager Suite. **D,** Binding of co-purified His-ULD/AB and the UCH domain of BAP1, as demonstrated by GST-UCH pull down with recombinant His-ULD/AB complex.

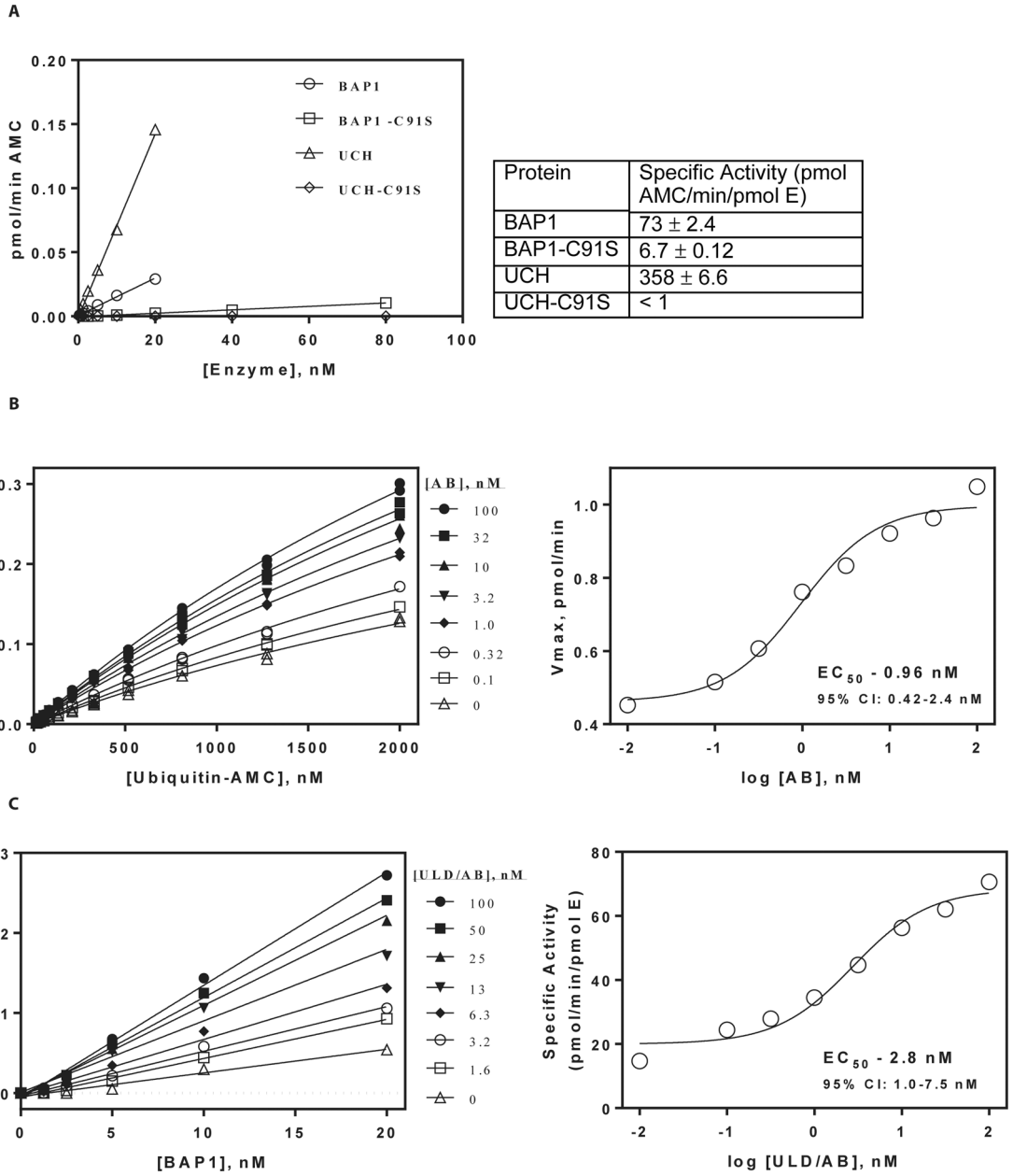

Protein	Specific Activity (pmol AMC/min/pmol E)
BAP1	73 ± 2.4
BAP1-C91S	6.7 ± 0.12
UCH	358 ± 6.6
UCH-C91S	< 1

Figure 3.

Activity of BAP1 and BAP1-UCH proteins as determined by cleavage of ubiquitin-7-amido-4-methylcoumarin (Ub-AMC). **A,** Cleavage of Ub-AMC mediated by full-length wild-type BAP1, full-length C91S BAP1 mutant, wild-type UCH domain of BAP1, or mutant C91S UCH domain. Enzymes were expressed in baculovirus with an N-terminal His-tag and purified using standard procedures. A range of concentrations for each enzyme was incubated with 100 nM Ub-AMC in 20 μL of 25 mM HEPES pH 7.4, 150 mM NaCl, 5 mM DTT and 0.005% Tween20 in 384-well plates. Fluorescence of free AMC was excited at 355 nm and emissions were measured at 460 nm at 2 min intervals. The resulting progress curves were fit to a straight line, and velocities were plotted against enzyme concentration to obtain specific activities. Effects of the AB box of ASXL2 and the ULD/AB complex of BAP1

mediated cleavage of Ub-AMC (**B, C**). **B,** Ub-AMC substrate titrations were incubated with full-length BAP1 (3 nM) in the presence of increasing concentrations of AB in assay buffer as described in Materials and Methods. The resulting progress curves were fit to a straight line (*left panel*), the velocities plotted against Ub-AMC concentration, and the data fit to the Michaelis-Menton equation. Potency of AB-mediated stimulation of maximal velocity of BAP1 (*right panel*). Each Vmax value was plotted against AB concentration, and the data fit to one-site dose response equation as described in the Materials and Methods. **C,** Full-length BAP1 was titrated in the presence of increasing concentrations of ULD/AB complex and 100 nM Ub-AMC in assay buffer, with resulting progress curves fit to a straight line, and velocities plotted against enzyme concentration to obtain specific activity (*left panel*). Potency of ULD/AB complex on specific activity of BAP1 (*right panel*). Slopes from panel C were plotted against ULD/AB concentration and the data fit to one-site dose response equation. All data points represent means of duplicate determinations from a single experiment, which was repeated twice.

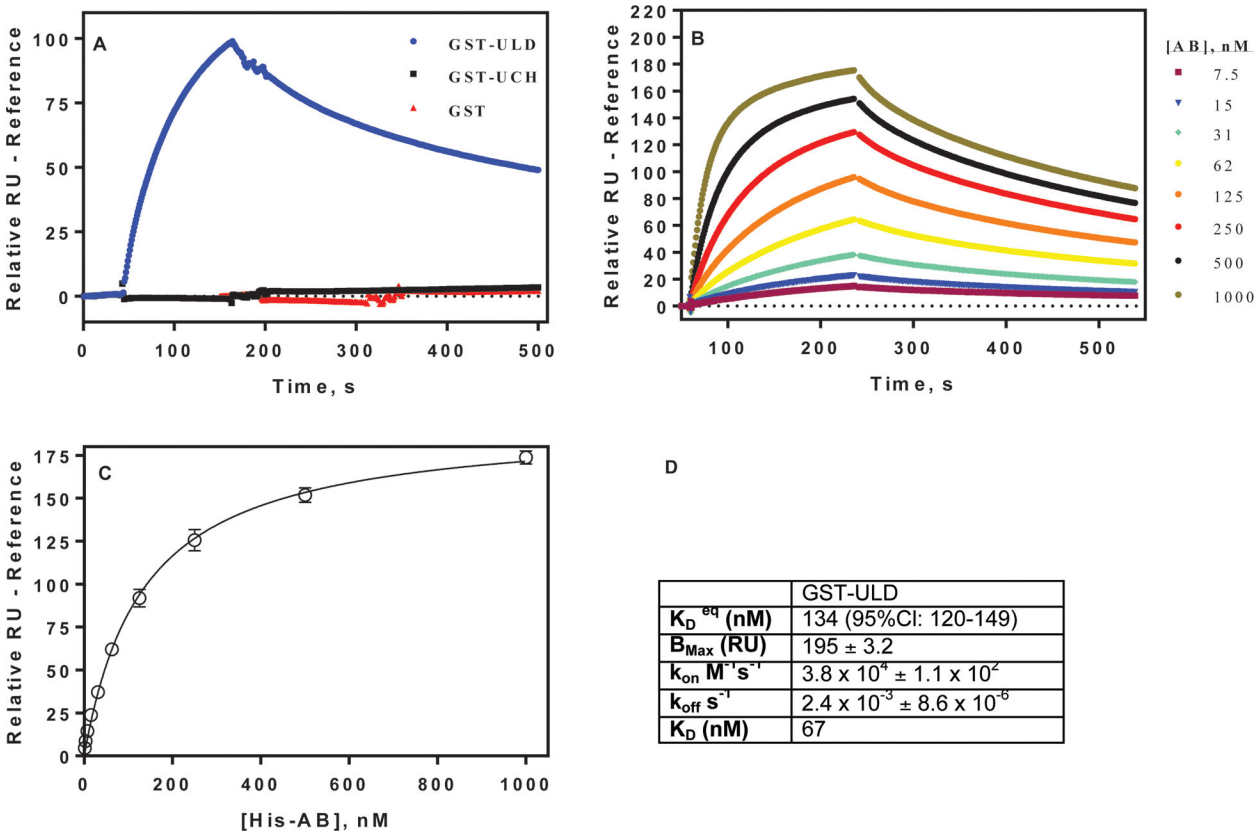

	GST-ULD
K_D^{eq} (nM)	134 (95%CI: 120-149)
B_{Max} (RU)	195 ± 3.2
k_{on} $M^{-1}s^{-1}$	$3.8 \times 10^{4} \pm 1.1 \times 10^{2}$
k_{off} s^{-1}	$2.4 \times 10^{-3} \pm 8.6 \times 10^{-6}$
K_D (nM)	67

Figure 4.

Characterization of binding of the ASXL2-AB box to the BAP1 ULD domain, as assessed by SPR. **A,** AB box (200 nM) binds to GST-tagged ULD domain of BAP1, but not to the UCH domain or GST alone. Data are means of duplicates +/− SEM. **B,** Kinetics of AB binding to GST-ULD. Kinetic parameters were determined from one-site binding model using Biacore evaluation software. Data represent means of duplicate determinations. **C,** Steady-state saturation binding curve of AB binding to ULD. K_D and B_{max} values were determined from one-site binding model in GraphPad Prism. Data points are the means +/− SEM of duplicate determinations. **D,** Equilibrium binding and kinetic parameters for interaction of AB and ULD determined in panels B and C.

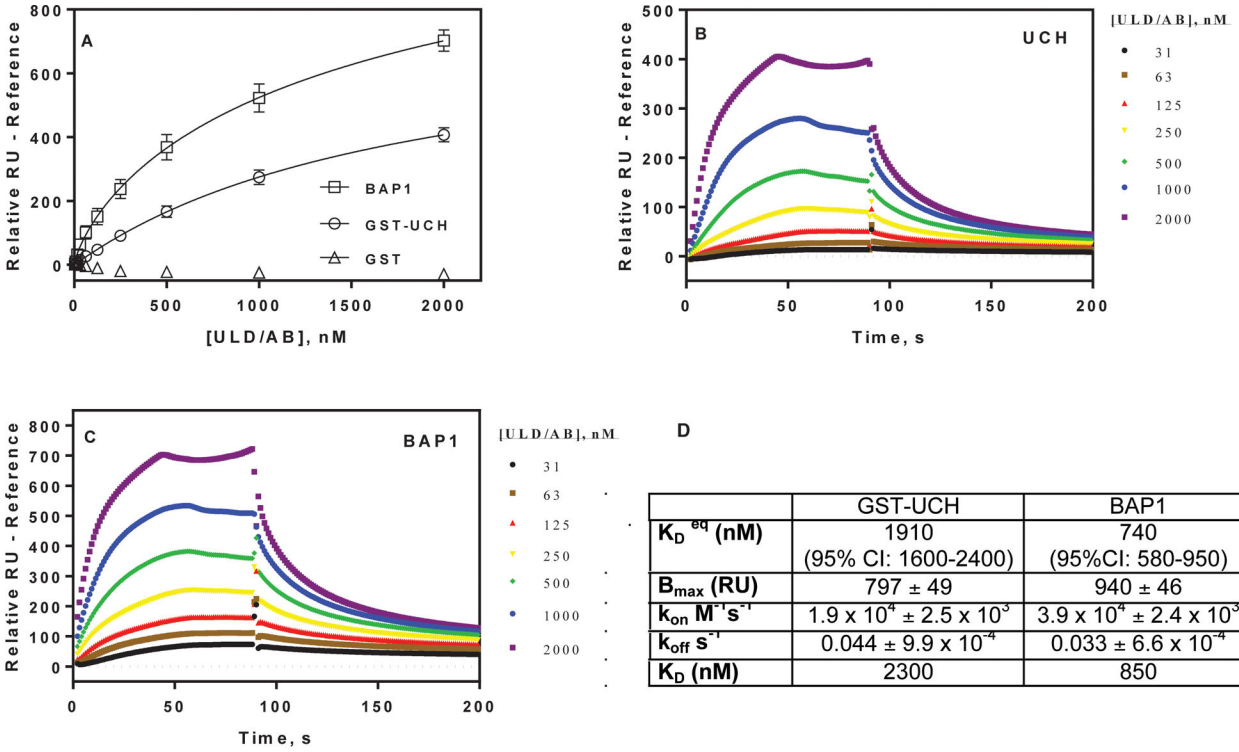

	GST-UCH	BAP1
K_D^{eq} (nM)	1910 (95% CI: 1600-2400)	740 (95%CI: 580-950)
B_{max} (RU)	797 ± 49	940 ± 46
k_{on} $M^{-1}s^{-1}$	$1.9 \times 10^4 \pm 2.5 \times 10^3$	$3.9 \times 10^4 \pm 2.4 \times 10^3$
k_{off} s^{-1}	$0.044 \pm 9.9 \times 10^{-4}$	$0.033 \pm 6.6 \times 10^{-4}$
K_D (nM)	2300	850

Figure 5.

Characterization of the binding of ULD/AB complex to BAP1 and BAP1-UCH domain as assessed by SPR. **A,** ULD/AB complex binds to UCH domain and full length BAP1 but not GST. Steady-state saturation binding curves fit to a one-site binding model. Data represent duplicate determinations +/− SEM. **B-C**, Kinetics of ULD/AB binding to UCH (**B**) and full-length BAP1 (**C**). Kinetic parameters determined from one-site binding model in Biacore evaluation software. Data represent means of duplicate determinations. **D,** Equilibrium binding and kinetic parameters for interaction of ULD/AB and UCH or full-length BAP1 as determined in panels A-C.

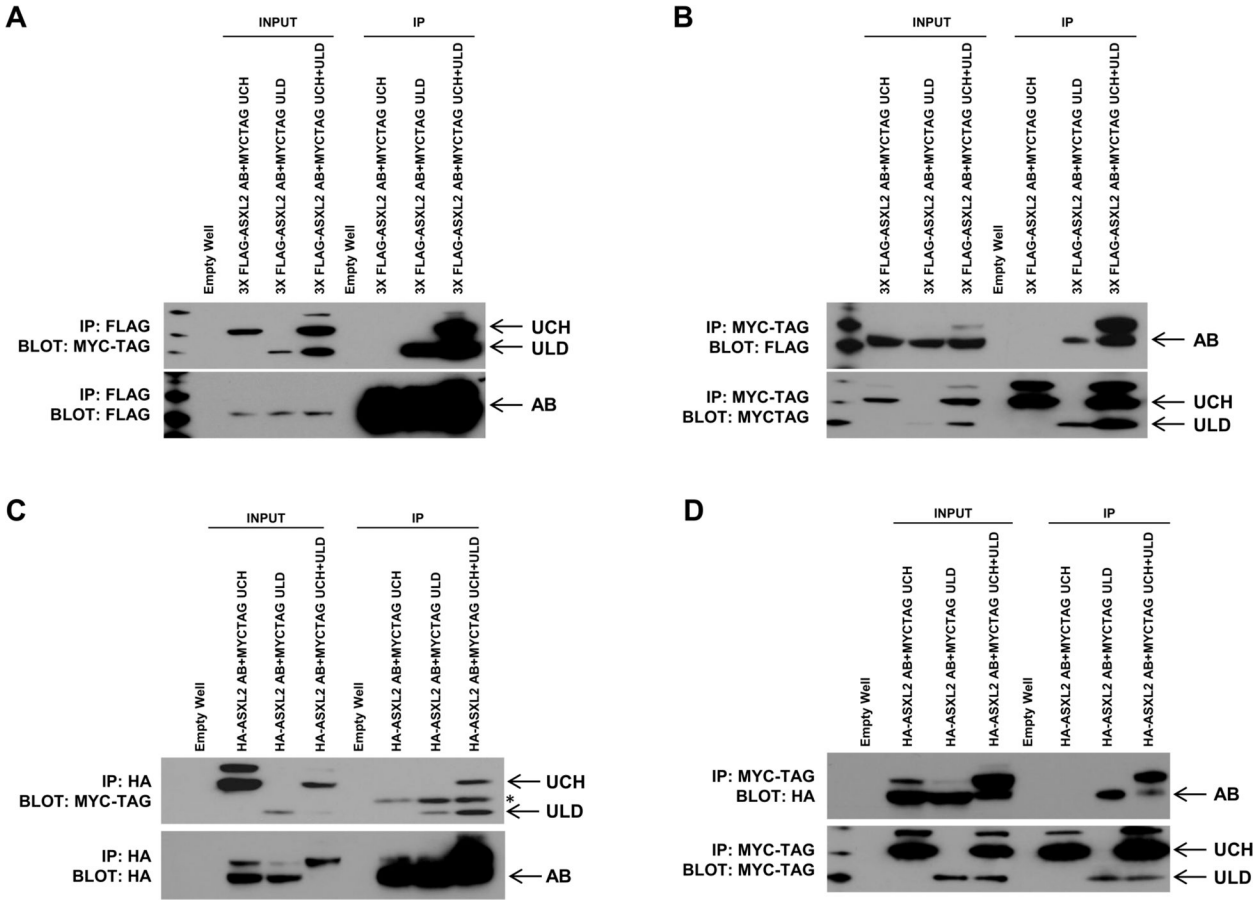

Figure 6.

Co-immunoprecipitation (co-IP) demonstrates that the BAP1-UCH, ULD and ASXL2-AB domains form a ternary stable complex in cells. HEK-293 cells were co-transfected or triple-transfected in different combinations with Myc-tag UCH and/or Myc-tag ULD domains of BAP1 and Flag-tag ASXL2-AB box. After 48 hours, samples were collected, and the co-IP assays were performed using Flag (**A**) and Myc-tag (**B**) antibodies coupled to agarose beads. The protein components in the complexes were detected by WB using Myc-tag antibody (**A**) or Flag antibody (**B**). In a parallel experiment, HEK-293 cells were co-transfected or triple-transfected in different combinations with Myc-tag UCH and/or Myc-tag ULD domains of BAP1 and HA-tag ASXL2-AB box. After 48 hours, the cell lysates were collected, and the co-IP assays were performed using HA-tag (**C**) and Myc-tag (**D**) antibodies coupled to agarose beads, the proteins were detected by WB using Myc-tag antibody (**C**) or HA antibody (**D**). Note that in panel C, asterisk (*) indicates non-specific light chain of anti-mouse secondary antibody. Collectively, these results demonstrate that the ASXL2-AB box does not bind to the BAP1 UCH domain alone, but it does bind to BAP1 ULD alone, and that the three proteins are pulled down as a stable AB-ULD-UCH ternary complex.

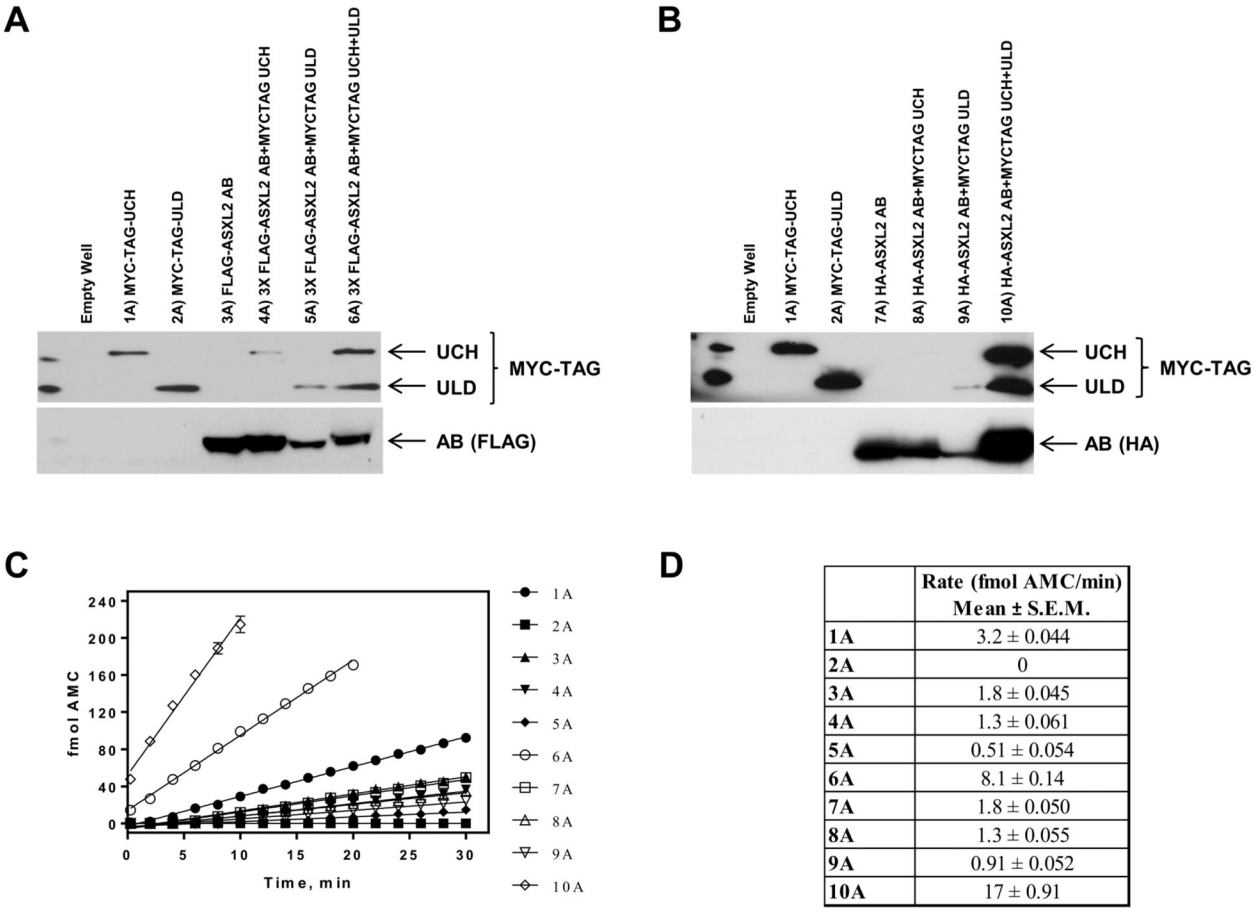

	Rate (fmol AMC/min) Mean ± S.E.M.
1A	3.2 ± 0.044
2A	0
3A	1.8 ± 0.045
4A	1.3 ± 0.061
5A	0.51 ± 0.054
6A	8.1 ± 0.14
7A	1.8 ± 0.050
8A	1.3 ± 0.055
9A	0.91 ± 0.052
10A	17 ± 0.91

Figure 7.

Immunoblotting after co-IP and elution of ASXL2-AB box and Myc-tag BAP1 domains and Ub-AMC assays performed using elutions from co-IP samples. HEK-293 cells were co-transfected or triple-transfected in different combinations with Myc-tag UCH and/or Myc-tag ULD domains of BAP1 and HA-tag ASXL2-AB box, and then co-IP assays were performed using the corresponding tag antibody for each tagged protein (**A, B**). Each single protein and interacting protein in the complex was eluted from the beads by competition with the corresponding synthetic peptide and purified (Myc-tag synthetic peptide for the UCH and ULD domains for single transfections, Flag (**A**) and HA (**B**) synthetic peptide for the AB box for single, co-transfected and triple-transfected cells). Eluted proteins in the complexes were detected by WB using antibodies specific for the different components (Myc-tag, Flag-tag, and HA-tag). Ub-AMC assays were performed using elutions from co-IP samples (**C, D**). Progress curves monitoring the cleavage of 100 nM Ub-AMC using dilutions of the co-IP elution samples that were chosen based upon densitometry analysis of the UCH band (**C**). Data points represent means ± S.E.M. of quadruplicate determinations. **D,** Rate of cleavage of Ub-AMC for each co-IP elution expressed as means ± S.E.M. The ASXL2-AB box binds to the ULD domain of BAP1 and mediates the formation of a tripartite complex consisting of AB, ULD, and UCH. Binding of the AB box to ULD

subsequently stabilizes the UCH structure, thereby increasing the catalytic activity of BAP1-UCH.